J|A|C|S
ARTICLES
Published on Web 01/24/2006

Strategies for Electrooptic Film Fabrication. Influence of Pyrrole−Pyridine-Based Dibranched Chromophore Architecture on Covalent Self-Assembly, Thin-Film Microstructure, and Nonlinear Optical Response

Antonio Facchetti,*,† Luca Beverina,‡ Milko E. van der Boom,§ Pulak Dutta,|| Guennadi Evmenenko,|| Atindra D. Shukla,§ Charlotte E. Stern,† Giorgio A. Pagani,*,‡ and Tobin J. Marks*,†

Contribution from the Department of Chemistry, Department of Physics and Astronomy, and the Materials Research Center, Northwestern University, Evanston, Illinois 60208-3113, Department of Material Science, University of Milano-Bicocca, via Cozzi 53, 20125 Milano, Italy, and Department of Organic Chemistry, The Weizmann Institute of Science, Rehovot, 76100, Israel

Received November 4, 2005; E-mail: a-facchetti@northwestern.edu; giorgio.pagani@mater.unimib.it; t-marks@northwestern.edu

Abstract: The new dibranched, heterocyclic "push−pull" chromophores bis{1-(pyridin-4-yl)-2-[2-(*N*-methylpyrrol-5-yl)]ethane}methane (**1**), 1-(pyrid-4-yl)-2-(*N*-methyl-5-formylpyrrol-2-yl)ethylene (**2**), {1-(*N*-methylpyridinium-4-yl)-2-[2-(*N*-methylpyrrol-5-yl)]ethane}{(1-(pyridin-4-yl)-2-[2-(*N*-methylpyrrol-5-yl)]ethane}-methane (**3**), *N*-methyl-2-[1-(*N*-methylpyrid-4-yl)ethen-2-yl]-5-[pyrid-4-yl]ethen-2-yl]pyrrole iodide (**4**), bis-{1-(*N*-methyl-4-pyridinio)-2-[2-(*N*-methylpyrrol-5-yl)]ethane}methane iodide (**5**), and *N*-methyl-2,5-[1-(*N*-methylpyrid-4-yl)ethen-2-yl]pyrrole iodide (**6**) have been synthesized and characterized. The neutral (**1** and **2**) and monomethyl salts (**3** and **4**) undergo chemisorptive reaction with iodobenzyl-functionalized surfaces to afford chromophore monolayers **SA-1**/**SA-2** and **SA-3**/**SA-4**, respectively. Molecular structures and other physicochemical properties have been defined by ^{1}H NMR, optical spectroscopy, and XRD. Thin-film characterization by a variety of techniques (optical spectroscopy, specular X-ray reflectivity, atomic force microscopy, X-ray photoelectron spectroscopy, and angle-dependent polarized second harmonic generation) underscore the importance of the chromophore molecular architecture as well as film growth method on film microstructure and optical/electrooptic response.

Introduction

Much attention has been recently devoted to the molecular engineering of silicon surfaces functionalized with organic thin films exhibiting specific electrical,[1] magnetic,[2] optical,[3] and electrooptic[4] properties as well as various combinations thereof.[5] These systems are potentially important for nanometer-scale miniaturization. Modulation of key surface bulk properties can be achieved both by proper molecular design and by fine control of the film structure at the molecular level.[6] However, predicting the molecular orientation and intermolecular interactions of a functional molecular assembly on a substrate surface remains a daunting challenge.[7] As far as nonlinear optical (NLO) and electrooptic (EO) materials are concerned,[8] many molecular design strategies and assembly methods have been devised to achieve polar order of the molecular building blocks on various substrates and within selected matrixes. Langmuir−Blodgett (LB) film transfer,[9] polymer/sol−gel electric field poling,[10] head-to-tail H-bonding,[11] crystal engineering,[12] and molecular self-assembly (SA)[4−6,13] are the most prominent examples. Of these, chemisorptive siloxane condensation yields densely packed intrinsically acentric organic films (i.e., organic mono-

† Department of Chemistry and the Materials Research Center, Northwestern University.
‡ Department of Material Science, University of Milano-Bicocca.
§ Department of Organic Chemistry, The Weizmann Institute of Science.
|| Department of Physics and Astronomy and the Materials Research Center, Northwestern University.

(1) (a) Cassoux, P.; Miller, J. S. in *Chemistry of Advanced Materials: An Overview*; Interrante, L. V., Hampden-Smith, M. J., Eds.; Wiley-VCH: New York, 1998; p 19. (b) Williams, J. M.; Ferraro, J. R.; Thorn, R. J.; Carlson, K. D.; Geiser, U.; Wang, H. H.; Kini, A. M.; Whangbo, M. H. *Organic Superconductors (Including Fullerenes)*; Prentice Hall: Englewood Cliffs, NJ, 1992. (c) Orlowski, G. A.; Chowdhury, S.; Long, Y.-T.; Sutherland, T. C.; Kraatz, H.-B *Chem. Commun.* **2005**, *10*, 1330. (d) Garcia, R.; Tello, M.; Moulin, J. F.; Biscarini, F. *Nano Lett.* **2004**, *4*, 1115. (e) Xie, X. N.; Chung, H. J.; Sow, C. H.; Wee, A. T. S. *Chem. Phys. Lett.* **2004**, *388*, 446. (f) Nuzzo, R. G. *Proc. Natl. Acad. Sci. U.S.A.* **2001**, *98*, 4827. (g) Special Issue on Molecular Conductors. *J. Mater. Chem.* **1995**, *10*, 5.

(2) (a) Condorelli, G. C.; Motta, A.; Fragalà, I. L.; Giannazzo, F.; Raineri, V.; Caneschi, A.; Gatteschi, D. *Angew. Chem., Int. Ed.* **2004**, *43*, 4081. (b) Kahn, O. *Molecular Magnetism*; VCH: Weinheim, 1993. (c) Teichert, C. *Appl. Phys. A: Mater. Sci. Proc.* **2003**, *76*, 653. (d) Sanz, N.; Terech, P.; Djurado, D.; Deme, B.; Ibanez, A. *Langmuir* **2003**, *19*, 3493. (e) Labuz, M.; Kuzma, M.; Wal, A. *Mater. Sci. Eng., C Biomimetic Supramol. Syst.* **2003**, *C23*, 945. (f) Miller, J. S.; Epstein, A. J. *Angew. Chem., Int. Ed. Engl.* **1994**, *33*, 385.

(3) (a) Zyss, J. *Molecular Nonlinear Optics: Materials, Physics and Devices*; Academic Press: Boston, 1994. (b) *Nonlinear Optics of Organic Molecules and Polymers*; Nalwa, H. S., Miyata, S., Eds.; CRC Press: New York, 1997. (c) Gulino, A.; Bazzano, S.; Condorelli, G. G.; Giuffrida, S.; Mineo, P.; Satriano, C.; Scamporrino, E.; Ventimiglia, G.; Vitalini, D.; Fragala, I. *Chem. Mater.* **2005**, *17*, 1079. (d) Friedrich, M.; Gavrila, G.; Himcinschi, C.; Kampen, T. U.; Kobitski, A. Yu; Mendez, H.; Salvan, G.; Cerrillo, I.; Mendez, J.; Nicoara, N.; Baro, A. M.; Zahn, D. R. T *J. Phys. Cond. Mater.* **2003**, *15*, S2699. (e) Lees, I. N.; Lin, H.; Canaria, C. A.; Gurtner, C.; Sailor, M. J.; Miskelly, G. M. *Langmuir* **2003**, *19*, 9812. (f) Optical Nonlinearities in Chemistry. Special issue of *Chem. Rev.* **1994**, *94*, 4 (1).

 10.1021/ja057556c CCC: $33.50

and multilayers) on hydroxylated substrates.[13] Formation of covalently bound optically functional molecular arrays on silicon and related surfaces is very attractive since the robust films can be readily integrated into diverse optical and electrooptic devices.[3,4] The molecular design of chromophores for such assembly schemes must strive to optimize: (i) coupling to the substrate surface, (ii) desired orientation of the chromophore dipole moment/β_{zz} direction, and (iii) bulk polar organization of the resulting films. For example, reaction of azine moieties with benzyl and alkyl halide functionalized surfaces is an effective approach to covalently graft azine-based chromophores to various hydroxylated substrates (e.g., glass, indium−tin oxide coated glass, silicon, plastics) while simultaneously creating a strongly π-accepting azinium group.[13l] It is expected that depending on the bond connectivity of the π-acceptor moiety with the π-donor group (through a π-conjugated bridge) and chromophore molecular geometrical arrangement on the substrate surface, various combinations of local molecular dipoles will generate different charge distributions on the substrate surface. The resulting bulk polarization determines the field of possible applications and potential interest. Active second-order NLO chromophores must have an asymmetric charge distribution, whereas symmetrical charge distributions usually enhance third-order NLO response.[14] The key importance of local dipole contributions to the resulting molecular hyperpolarizability of di/multibranched chromophores has been studied theoretically and experimentally[15] with predicted/measured enhancements of

(4) (a) *Organic Thin Films for Waveguiding Nonlinear Optics*; Kajzar, F., Swalen, J. D., Eds.; Gordon and Breach Publishers: Langhorne, PA, 1996. (b) Prasad, P. N.; William, D. J. *Introduction to Nonlinear Optical Effects in Molecules and Polymers*; Wiley: New York, 1991. (c) Haller, M. A.; Lawson, R.; Clot, O.; Sherwood, T.; Dalton, L.; Jen, A. K. *Proc. SPIE* **2003**, 5212 (Linear and Nonlinear Optics of Organic Materials III), 326. (d) Gu, C.; Xu, Y.; Liu, Y.; Pan, J. J.; Zhou, F.; He, H. *J. Opt. A: Pure Appl. Opt.* **2003**, *5*, S420. (e) Enami, Y.; Meredith, G.; Peyghambarian, N.; Jen, A. K.-Y *Appl. Phys. Lett.* **2003**, *83*, 4692. (f) Hou, Z.; You, W.; Yu, L. *Appl. Phys. Lett.* **2003**, *82*, 3385. (g) Lee, M.; Katz, H. E.; Erben, C.; Gill, D. M.; Gopalan, P.; Heber, J. D.; McGee, D. J. *Science* **2002**, *298*, 1401. (h) van der Boom, M. E. *Angew. Chem., Int. Ed.* **2002**, *18*, 3363. (i) Würthner, F.; Wortmann, R., Meerholz, K *ChemPhysChem* **2002**, *3*, 17. (h) Zhao, Y.-G.; Wu, A.; Lu, H.-L.;Chang, S.; Lu, W.-K.; Ho, S.-T.; van der Boom, M. E.; Malinsky, J. E.; Marks, T. J. *Appl. Phys. Lett.* **2001**, *79*, 587−589. (k) Enami, Y.; Poyhonen, P.; Mathine, D. L.; Bashar, A.; Madasamy, P.; Honkanen, S.; Kippelen, B.; Peyghambarian, N.; Marder, S. R.; Jen, A. K−Y.; Wu, J *Appl. Phys. Lett.* **2000**, *76*, 1086. (l) Robinson, B. H.; Dalton, L. R.; Harper, A. W.; Ren, A.; Wang, F.; Zhang, C.; Todorova, G.; Lee, M.; Aniszfeld, R.; Garner, S.; Chen, A.; Steier, W. H. Houbrecht, S.; Persoons, A.; Ledoux, I.; Zyss, J.; Jenn, A. K. *Chem. Phys.* **1999**, *245*, 35. (m) Marder, S. R.; Kippelen, B.; Jen, A. K. Y.; Peyghambarian, N. *Nature* **1997**, *388*, 845.

(5) (a) Shirahata, N.; Shin, W.; Murayama, N.; Hozumi, A.; Yokogawa, Y.; Kameyama, T.; Masuda, Y.; Koumoto, K. *Adv. Funct. Mater.* **2004**, *14*, 580. (b) Averseng, F.; Lepetit, C.; Lacroix, P. G.; Tuchagues, J.-P. *Chem. Mater.* **2000**, *12*, 2225. (c) Malfant, I.; Cordente, N.; Lacroix, P. G.; Lepetit, C. *Chem. Mater.* **1998**, *10*, 4079. (d) Bernard, S.; Yu, P.; Coradin, T.; Rivière, E.; Nakatani, K.; Clement, R. *Adv. Mater.* **1997**, *9*, 981. (e) Lacroix P. G.; Nakatani, K. *Adv. Mater.* **1997**, *9*, 1105. (f) Kurmoo, M.; Graham, A. W.; Day, P.; Coles, S. J.; Hursthouse, M. B.; Caulfield, J. L.; Singleton, J.; Pratt, F. L.; Hayes, W.; Ducasse L.; Guionneau, P. *J. Am. Chem. Soc.* **1995**, *117*, 12209. (g) Clement, R.; Lacroix, P. G.; O'Hare D.; Evans, J. *Adv. Mater.* **1994**, *6*, 794. (h) Lacroix, P. G.; Clement, R.; Nakatani, K.; Zyss J.; Ledoux, I. *Science* **1994**, *263*, 658. (i) Goze, F.; Laukhin, V. N.; Brossard, L.; Audouard, A.; Ulmet, J. P.; Askenazy, S.; Naito, T.; Kobayashi, H.; Kobayashi M.; Cassoux, P. *Europhys. Lett.* **1994**, *28*, 427. (j) Sutter, K.; Hulliger J.; Gunter, P. *Solid State Commun.* **1990**, *74*, 867.

(6) (a) Gershewitz, O.; Grinstein, M.; Sukenik, Chaim N.; Regev, Keren; Ghabboun, Jamal; Cahen, David. *J. Phys. Chem. B* **2004**, *108*, 664. (b) Vilan, A.; Shanzer, A.; Cahen, D. *Nature* **2000**, *404*, 166. (c) Bruening, M.; Cohen, R.; Guillemoles, J. F.; Moav, T.; Libman, J.; Shanzer, A.; Cahen, D. *J. Am. Chem. Soc.* **1997**, *119*, 5720.

(7) (a) Yerushalami, R.; Scherz, A.; van der Boom, M. E. *J. Am. Chem. Soc.* **2004**, *126*, 2700. (b) Di Bella, S.; Fragala, I.; Leonardi, N.; Sortino, S *Inorg. Chim. Acta* **2004**, *357*, 3865. (c) Klare, J. E.; Tulevski, G. S.; Sugo, K.; de Picciotto, A.; White, K. A.; Nuckolls, C *J. Am. Chem. Soc.* **2003**, *125*, 6030. (d) Kmetko, J.; Datta, A.; Evmenenko, G.; Durbin, M. K.; Richter, A. G.; Dutta, P *Langmuir* **2001**, *17*, 4697. (e) Benítez, I. O.; Bujoli, B.; Camus, L. J.; Lee, C. M.; Odobel, F.; Talham, D. R. *J. Am. Chem. Soc.* **2002**, *124*, 4363. (f) Kuzmenko, I.; Rapaport, H.; Kjaer, K.; Als-Nielsen, J.; Weissbuch, I.; Lahav, M.; Leiserowitz, L. *Chem. Rev.* **2001**, *101*, 1659.

(8) (a) Cariati, E.; Roberto, D.; Ugo, R.; Ford, P. C.; Galli, S.; Sironi, A. *Inorg. Chem* **2005**, *44*, 4077. (b) Tamm, M.; Bannenberg, T.; Baum, K.; Frohlich, R.; Steiner, T.; Meyer-Friedrichsen, T.; Heck, J *Eur. J. Inorg. Chem.* **2000**, *6*, 1161. (c) Hu, Z.-Y.; Fort, A.; Barzoukas, M.; Jen, A. K.-Y.; Barlow, S.; Marder, S. R. *J. Phys. Chem* **2004**, *108*, 8626. (d) Dalton, L. R.; Robinson, B. H.; Nielson, R.; Jen, A. K.; Casmier, D.; Rabiei, P.; Steier, W. H. *SPIE Proc.* **2003**, *4991*, 508. (e) Pereverzev, Y. V.; Prezhdo, O. V.; Dalton, L. R. *Chem. Phys. Lett.* **2003**, *373*, 207. (f) Lanata, M.; Bertarelli, C.; Gallazzi, M. C.; Bianco, A.; Del Zoppo, M.; Zerbi, G. *Synth. Met.* **2003**, *138*, 357. (g) You, W.; Cao, S.; Hou, Z.; Yu, L. *Macromolecules* **2003**, *36*, 7014. (h) Qin, A.; Bai, F.; Ye, C. *Theochem* **2003**, *631*, 79. (i) Ushiwata, T.; Okamoto, E.; Komatsu, K.; Kaino, T.; Jen, A. K.-Y. *Opt. Mater.* **2003**, *21*, 61. (j) P. G. Lacroix *Eur. J. Inorg. Chem.* **2001**, 339. (k) Lemaître, N.; Attias, A.-J.; Ledoux, I.; Zyss, J. *Chem. Mater.* **2001**, *13*, 1420−1427. (l) Würthner, F.; Yao, S.; Schilling, J.; Wortmann, R.; Redi-Abshiro, M.; Mecher, E.; Gallego-Gomez, F.; Meerholz, K. *J. Am. Chem. Soc.* **2001**, *123*, 2810. (m) Rekaï, E. D.; Baudin, J.-B.; Jullien, L.; Ledoux, I.; Zyss, J.; Blanchard-Desce, M. *Chemistry* **2001**, *7*, 4395. (n) Bublitz, G. U.; Ortiz, R.; Runser, C.; Fort, A.; Barzoukas, M.; Marder, S. R.; Boxer, S. G. *J. Am. Chem. Soc.* **1997**, *119*, 2311. (o) Alheim, M.; Barzoukas M.; Bedworth, P. V.; Blanchard-Desce, M.; Fort, A.; Hu, Z.-Y.; Marder, S. R.; Perry, J. W.; Runser, C.; Staehelin, M.; Zysset, B. *Science* **1996**, *271*, 335. (p) Marder, S. R.; Perry, J. W.; Bourhill, G.; Gorman, C. B.; Tiemann, B. G.; Mansour, K. *Science* **1993**, *261*, 186.

(9) (a) Kim, H. S.; Lee, S. M.; Ha, K.; Jung, C.; Lee, Y.-J.; Chun, Y. S.; Kim, D.; Rhee, B. K.; Yoon, K. B. *J. Am. Chem. Soc.* **2004**, *126*, 673. (b) Ashwell, G. J.; Paxton, G. A. N. *Austr. J. Chem.* **2002**, *55*, 199. (c) Ashwell, G. J. *J. Mater. Chem.* **1999**, *9*, 1991. (d) Ricceri, R.; Abbotto, A.; Facchetti, A.; Grando, D.; Gabrielli, G.; Pagani, G. A. *Colloids Surf., A* **1999**, *150*, 289. (e) Ricceri, R.; Neto, C.; Abbotto, A.; Facchetti, A.; Pagani, G. A. *Langmuir* **1999**, *15*, 2149. (f) Roberts, M. J.; Lindsay, G. A.; Herman, W. N.; Wynne, K. J. *J. Am. Chem. Soc.* **1998**, *120*, 11202. (g) Wijekoon, W. M. K. P.; Wijayu, S. K.; Bhawalkar, J. D.; Prasad, P. N.; Penner, T. L.; Armstrong, N. J.; Ezenyilimba, M. C.; Williams, D. J. *J. Am. Chem. Soc.* **1996**, *118*, 4480.

(10) (a) Gray, T.; Overney, R. M.; Haller, M.; Luo, J.; Jen, A. K.-Y. *Appl. Phys. Lett.* **2005**, *86*, 211908/1. (b) Dalton, L. R.. *Pure Appl. Chem.* **2004**, *76*, 1421. (c) Sinyukov, A. M.; Leahy, M. R.; Hayden, L.; Michael, H., Marnie; Luo, J.; Jen, A. K.-Y.; Dalton, L. R. *Appl. Phys. Lett.* **2004**, *85*, 5827. (d) Firestone, K. A.; Reid, P.; Lawson, R.; Jang, S.-H.; Dalton, L. R. *Inorg. Chim. Acta* **2004**, *357*, 3957. (e) Luo, J.; Liu, S.; Haller, M.; Liu, L.; Ma, H.; Jen, A. K.-Y. *Adv. Mater.* **2002**, *14*, 1763. (f) Shi, Y.; Zhang, C.; Zhang, H.; Bechtel, J. H.; Dalton, L. R.; Robinson, B. H.; Steier, W. H. *Science* **2000**, *288*, 199. (g) Yitzchaik, S.; Di Bella, S.; Lundquist, P. M.; Wong, G. K.; Marks, T. J. *J. Am. Chem. Soc.* **1997**, *119*, 2995.

(11) (a) Zhu, P.; Kang, H.; Facchetti, A.; Evmenenko, G.; Dutta, P.; Marks, T. J. *J. Am. Chem. Soc.* **2003**, *125*, 11496. (b) Barth, J. V.; Weckesser, J.; Trimarchi, G.; Vladimirova, M.; De Vita, A.; Cai, C.; Brune, H.; Güenter, P.; Kern, K. *J. Am. Chem. Soc.* **2002**, *124*, 7991. (c) Saadeh, H.; Wang, L.; Yu, L. *J. Am. Chem. Soc.* **2000**, *122*, 546. (d) Pan, J.; Chen, M.; Warner, W.; He, M.; Dalton, L.; Hogen-Esch, T. E. *Macromolecules* **2000**, *33*, 7835. (e) Barth, J. V.; Weckesser, J.; Cai, C.; Günter, P.; Burgi, L.; Jeandupeux, O.; Kern, K. *Agnew. Chem., Int. Ed. Engl.* **2000**, *39*, 1230. (f) Cai, C.; Müller, B.; Weckesser, J.; Barth, J. V.; Tao, Y.; Bosch, M. M.; Kundig, A.; Bosshard, C.; Biaggio, I.; Günter, P. *Adv. Mater.* **1999**, *11*, 745. (g) Müller, B.; Cai, C.; Kundig, A.; Tao, Y.; Bosch, M.; Jager, M.; Bosshard, C.; Günter, P. *Appl. Phys. Lett.* **1999**, *74*, 3110. (h) Johal, M. S.; Cao, Y. W.; Chai, X. D.; Smilowitz, L. B.; Robinson, J. M.; Li, T. J.; McBranch, D.; Li, D. Q. *Chem. Mater.* **1999**, *11*, 1962. (i) Cai, C.; Boesch, M. M.; Tao, Y.; Müeller, B.; Gan, Z.; Kuendig, A.; Bosshard, C.; Liakatas, I.; Jaeger, M.; Güenter, P. *J. Am. Chem. Soc.* **1998**, *120*, 8563.

(12) Evans, O. R.; Lin, W. *Acc. Chem. Res.* **2002**, *35*, 511.

(13) (a) van der Boom, M. E.; Evmenenko, G.; Yu, C.; Dutta, P.; Marks, T. J. *Langmuir* **2003**, *19*, 10531. (b) Johal, M. S.; Casson, J. L.; Chiarelli, P. A.; Liu, D.-G.; Shaw, J. A.; Robinson, J. M.; Wang, H.-L. *Langmuir* **2003**, *19*, 8876. (c) Claus, R.; Wang, Y.-X.; Zhang, L.; Cooper, K. *Multilayer Thin Films* **2003**, 461. (d) Zhu, P.; van der Boom, M. E.; Kang, H.; Evmenenko, G.; Dutta, P.; Marks, T. J. *Chem. Mater.* **2002**, *14*, 4982. (e) van der Boom, M. E.; Zhu, P.; Evmenenko, G.; Malinsky, J. E.; Lin, W.; Dutta, P.; Marks, T. J. *Langmuir* **2002**, *18*, 3704. (f) van der Boom, M. E.; Evmenenko, G.; Dutta, P.; Marks, T. J. *Adv. Funct. Mater.* **2001**, *11*, 393. (g) Neff, G. A.; Helfrich, M. R.; Clifton, M. C.; Page, C. J. *Chem. Mater.* **2000**, *12*, 2363−2371. (h) Flory, W. C.; Mehrens, S. M.; Blanchard, G. J. *J. Am. Chem. Soc.* **2000**, *122*, 7976. (i) Hung, W.; Helvenston, M.; Casson, J. L.; Wang, R.; Bardeau, J.-F.; Lee, Y.; Johal, M. S.; Swanson, B. I.; Robinson, J. M.; Li, D.-Q. *Langmuir* **1999**, *15*, 6510. (j) Hanken, D. G.; Naujok, R. R.; Gray, J. M.; Corn, R. M. *Anal. Chem.* **1997**, *69*, 240−248. (k) Lin, W.; Lee, T.-L.; Lyman, P. F.; Lee, J.; Bedzyk, M. J.; Marks, T. J. *J. Am. Chem. Soc.* **1997**, *119*, 2205. (l) Lin, W.; Lin, W.; Wong, G. K.; Marks, T. J. *J. Am. Chem. Soc.* **1996**, *118*, 8034. (m) Yitzchaik, S.; Marks, T. J. *Acc. Chem. Res.* **1996**, *29*, 197. (n) Katz, H. E.; Wilson, W. L.; Scheller, G. *J. Am. Chem. Soc.* **1994**, *116*, 6636.

(14) (a) *Molecular Nonlinear Optics*; Zyss, J., Ed.; Academic Press: New York, 1994. (b) Barlow, S.; Risko, C.; Coropceanu, V.; Tucker, N. M.; Jones, S. C.; Levi, Z.; Khrustalev, V. N.; Antipin, M. Y..; Kinnibrugh, T. L.; Timofeeva, T.; Marder, S. R.; Bredas, J.-L *Chem. Commun.* **2005**, 764. (c) Thomas, J.; Fuentes-Hernandez, C.; Yamamoto, M.; Cammack, K.; Matsumoto, K.; Walker, G. A.; Barlow, S.; Kippelen, B.; Meredith, G.; Marder, S. R.; Peyghambarian, N. *Adv. Mater.* **2004**, *16*, 2032.

the second-order molecular response coefficient (β) values of more than one order of magnitude. However, to the best of our knowledge, there have been no reports of achieving self-assembly of these kinds of molecules.

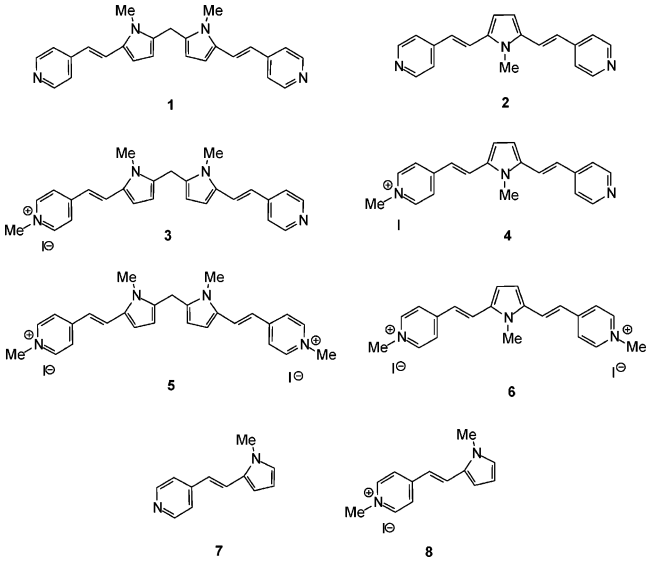

We recently reported that heterocyle-based dyes composed of both π-excessive (pyrrole, indole, thiophene) and π-deficient (pyridine, diazines, quinoline, isoquinoline) heteroaromatics afford new chromophore families exhibiting both second- and third-order response.[16] The combination of a pyridinium salt and a pyrrol-2-yl substituent results in highly effective "push−pull" systems. We now present here a novel class of dibranched chromophores based on such heterocycle combinations bridged by ethylene or methylene moieties and which underscore the consequences of molecule structure on self-assembled thin-film microstructure and optical/EO response. The parent molecules **1** and **2** contain two terminal pyridyl rings which undergo reaction with benzyl halide-functionalized surfaces in a consecutive fashion. The charge distribution of the resulting siloxane-based films is dominated by the molecular structure of the chromophore precursor and is switched on by the benzyl halide coupling layer. The molecular orientation, film microstructure, and linear/nonlinear optical properties are studied by a combination of techniques, including X-ray reflectivity (XRR), atomic force microscopy (AFM), X-ray photoelectron spectroscopy (XPS), optical spectroscopy, and second-harmonic generation (SHG) spectroscopy. Furthermore, stepwise alkylation of compounds **1** and **2** in solution affords mono- (**3**, **5**) and dialkylated (**4**, **6**) chromophore salts (Scheme 2). These new compounds provide additional insight into the reactivity of the bidentate precursors **1** and **2** toward iodobenzyl-functionalized surfaces and their unique reactivity patterns vis-à-vis formally monomeric chromophore precursors **7** and **8**.

Results and Discussion

Synthesis of the Chromophores 1−6 and Film Fabrication. We recently reported that the reaction of compound **7** with $(CH_2O)_x$ and diethanolamine (R_2NH, R = $-CH_2CH_2OH$) in the presence of *p*-toluenesulfonic acid in dry EtOH results in the formation of diethanolamine-functionalized chromophore **9** (path I, Scheme 1). This chromophore is a key building block for the preparation of all-heterocyclic-based intrinsically acentric siloxane-based multilayers.[16a]

In contrast to these results, reaction of compound **7** with $(CH_2O)_x$ and diethanolamine (or dibutylamine) in the presence of *p*-toluenesulfonic acid in an EtOH/H_2O mixture (1:1 v/v) results in the formation of the new dimeric chromophore **1** (path II). Although detailed mechanistic studies were not carried out, it is likely that intermediate **A** undergoes nucleophilic attack on the Schiff's base carbon by the electron-rich pyrrole moiety of **7**, forming undetected pyrrolium salt **B**. The latter would then undergo intramolecular amine-assisted proton rearrangement (Scheme 1). Hydrolysis of the resulting amine salt **C** affords intermediate **D**, which is followed by loss of H_2O and formation of postulated methylenepyrrolium salt **E**. Intermediate **E** then undergoes nucleophilic attack by the pyrrole moiety of **7** at the terminal olefinic carbon, yielding methylene-bridged dimer **1**, which is isolated in high yield. Monomethylated *N*-methylpyridinium salt **3** was prepared by quaternization of precursor **1** with MeI in $CHCl_3$. The dimethyliodide salt **5** was likewise prepared by treatment of **1** or **3** with MeI in a sealed tube in CH_3CN at 110 °C.

Chromophore precursor **2** was prepared as shown in Scheme 3. Direct formylation of **7** results in the formation of a variety of products, perhaps due to interaction of the pyridine nitrogen with the immonium $POCl_3$−DMF adduct. Since Vilsmeier condensation occurs under neutral or acidic reaction conditions, the pyridine moiety was protected by converting it to the corresponding pyridinium salt **10** using a stoichiometric amount of HBF_4 in ethanol. Formylation of **10** according to Vilsmeier protocol then cleanly affords chromophore **11** in 75% yield. Subsequent aldol condensation of **11** with the picolinate anion (from reaction of 4-picoline with excess of NaH) in anhydrous DMF affords chromophore precursor **2** in 60% yield. Recrystallization from water or alcohol yields analytically pure **2**. Reaction of **11** with a stoichiometric amount of *N*-methyl-4-picolinium iodide in refluxing ethanol, in the presence of piperidine, yields **4** as a blue-violet solid. Treatment of **2** with a 2-fold excess of MeI in refluxing ethanol for 2 h finally affords bis-quaternized chromophore **6** as a dark-blue precipitate. All of the new chromophores and chromophore precursors were characterized by conventional spectroscopic and analytical methodologies as described below.

The formation of pyridinium-based chromophore films (**SA-1**−**SA-4**) was achieved via a two-step, self-limiting chemisorptive siloxane condensation process as shown in Scheme 4. In

(15) (a) Katan, C.; Terenziani, F.; Mongin, O.; Werts, M. H. V.; Porres, L.; Pons, T.; Mertz, J.; Tretiak, S.; Blanchard-Desce, M. *J. Phys. Chem. A* **2005**, *109*, 3024. (b) Curreli, S.; Deplano, P.; Faulmann, C.; Ienco, A.; Mealli, C.; Mercuri, M. L.; Pilia, L.; Pintus, G.; Serpe, A.; Trogu, E. F. *Inorg. Chem.* **2004**, *43*, 5069. (c) Senechal, K.; Maury, O.; Le Bozec, H.; Ledoux, I.; Zyss, J. *J. Am. Chem. Soc.* **2002**, *124*, 4560. (d) Reyes-Esqueda, J.; Darracq, B.; Garcia-Macedo, J.; Canva, M.; Blanchard-Desce, M.; Chaput, F.; Lahlil, K.; Boilot, J. P.; Brun, A.; Levy, Y. *Optics Commun.* **2001**, *198*, 207. (e) Di Bella, S.; Fragala, I.; Ledoux, I.; Zyss, J. *Chemistry* **2001**, *7*, 3738. (f) Kay, A. J.; Woolhouse, A. D.; Gainsford, G. J.; Haskell, T. G.; Barnes, T. H.; McKinnie, I. T.; Wyss, C. P. *J. Mater. Chem.* **2001**, *11*, 996. (g) Asha, S. K.; Kavita, K.; Das, P. K.; Ramakrishnan, S. *Chem. Mater.* **1999**, *11*, 3352. (h) Goodson, T., III; Wang, C. H. *Macromolecules* **1993**, *26*, 1837.

(16) (a) Facchetti, A.; Abbotto, A.; Beverina, L.; Bradamante, S.; van der Boom, M. E.; Evmenenko, G.; Dutta, P.; Marks, T. J.; Pagani, G. A. *Chem. Mater.* **2003**, *15*, 1064. (b) Abbotto, A.; Beverina, L.; Bradamante, S.; Facchetti, A.; Klein, C.; Pagani, G. A.; Abshiro, M. R.; Wortmann, R. D. *Chem. Eur. J.* **2003**, *9*, 1991. (c) Abbotto, A.; Beverina, L.; Bradamante, S.; Facchetti, A.; Pagani, G. A.; Bozio, R.; Ferrante, C.; Pedon, D.; Signorini, R. *Synth. Met.* **2003**, *139*, 795. (d) Abbotto, A.; Beverina, L.; Bozio, R.; Facchetti, A.; Ferrante, C.; Pagani, G. A.; Pedron, D.; Signorini, R. *Chem. Commun.* **2003**,*17*, 2144.

Scheme 1. Synthetic Route to and Proposed Mechanism for the Formation of Prechromophore Dimer **1**

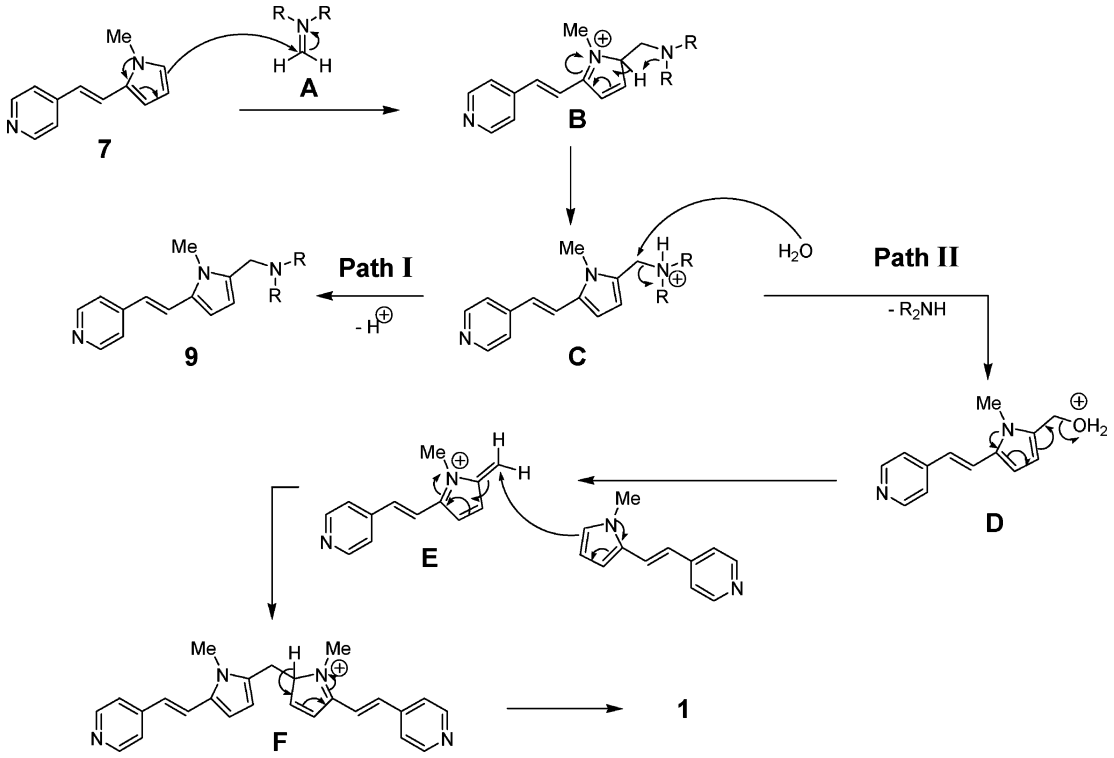

Scheme 2. Synthesis of Chromophores **3** and **5** by Alkylation of **1** with MeI

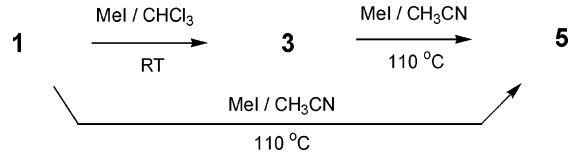

the first step, hydroxylated substrates undergo reaction with the *p*-(iodomethyl)phenyldiiodochlorosilane (**IBnS**) coupling reagent in solution to afford the benzyl halide functionalized monolayer **SA-IBnS**. The film quality was verified by AFM and advancing aqueous contact angle measurements. Quaternization at the pyridyl moieties of chromophore precursors **1**−**4** with the benzyl-halide terminated substrate surface (**SA-IBnS**) can be accomplished via either a vapor- or solution-phase procedure. In the vapor deposition process, films of **1**−**4** are spin-coated on the **SA-IBnS** substrates and the samples heated in a vacuum oven at 100−130 °C (15 Torr). In the solution deposition method, the benzyl halide functionalized substrates are immersed in dry solutions of **1**−**4** and heated at 90 °C in a sealed pressure reactor for ∼12 h.

The first procedure is more rapid and yields films of higher quality as indicated by UV−vis and SHG measurements (see below). Attempts to improve the film quality from the solution method by changing solvent and reaction time and temperature were performed, but the results were not satisfactory. Furthermore, increase reaction time results in the formation of particulates contaminating the substrates. Therefore, subsequent film microstructural characterization was performed solely on the vapor-deposited films. The chromophoric films strongly adhere to the hydrophilic substrates, cannot be detached by the conventional "Scotch tape" decohesion test,[17] and are insoluble in common organic solvents. The proposed molecular architectures of chromophoric films **SA-1**−**SA-4** depicted in Scheme

Scheme 3. Synthesis of Compounds **2**, **4**, and **6**

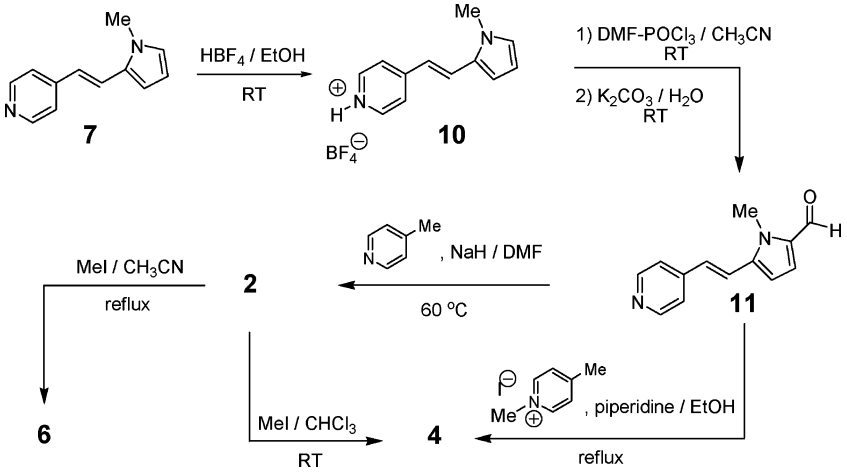

Scheme 4. Schematic Representation of Covalent-Assembled Films of Chromophores **1**−**4**[a]

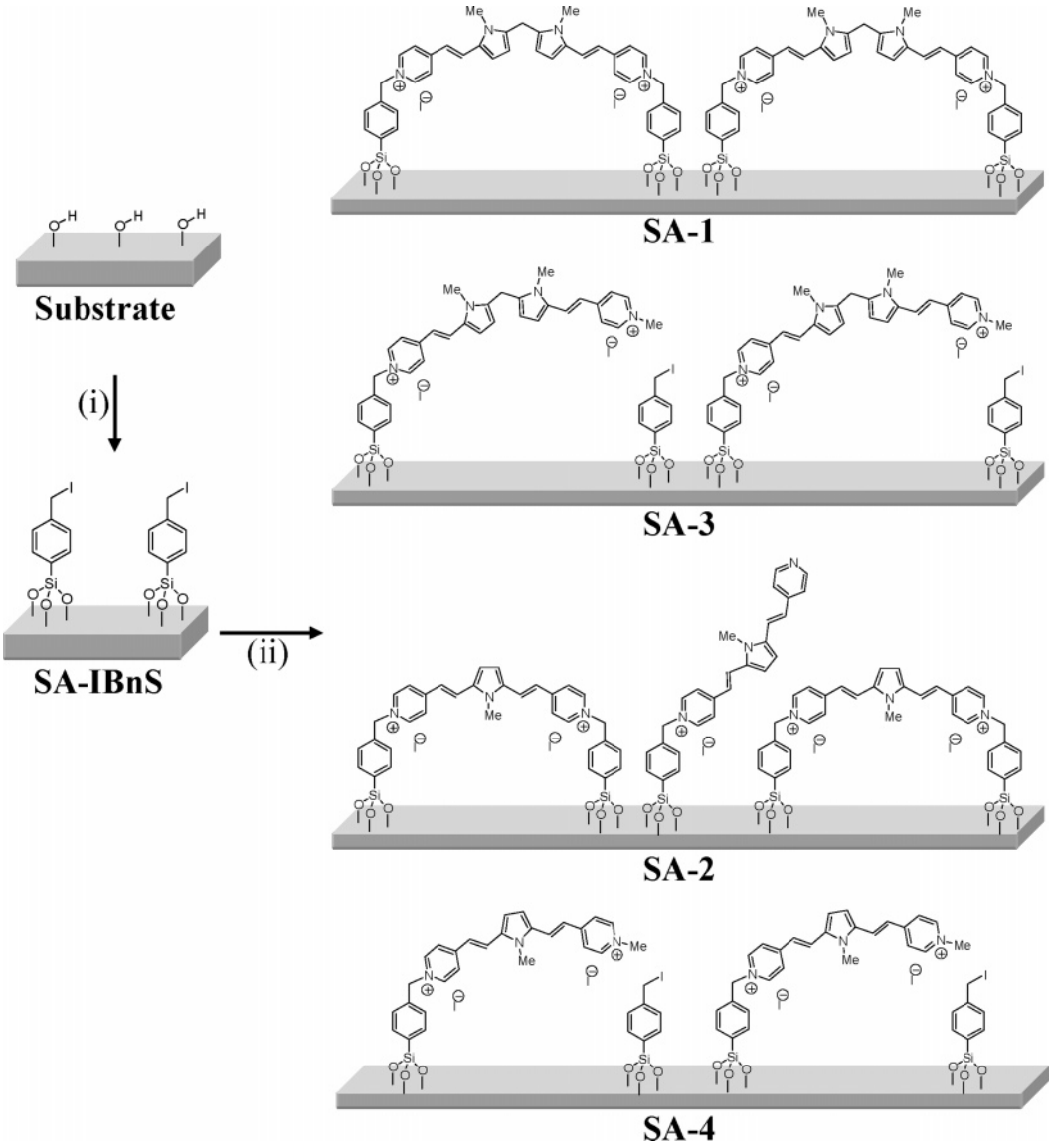

[a] Key: (i) SA of the coupling reagent; (ii) SA of chromophore precursors **1**−**4**.

4 are deduced from a combination of techniques (vide infra) which demonstrate the formation of dense films σ-bonded to the functionalized substrate surface.

Chromophore Structural Characterization. The structures of **1** and of the corresponding methylated salts **3** and **5** were established by elemental analysis, UV−vis measurements, and ^{1}H NMR spectroscopy. The symmetric compound **1** exhibits a single set of resonances in the ^{1}H NMR for the two identical pyridine-C═C-pyrrole moieties (Figure 1A). Alkylation of only one of the two pyridine nitrogens disrupts the molecular symmetry, and the ^{1}H NMR spectrum now exhibits two sets of resonances. The set of signals associated with the alkylated moiety is shifted to low field, because of the positive charge on the pyridinium ring. The resonances of the neutral pyridine-pyrrole fragment are unaffected, demonstrating that the methylene spacer is an excellent insulator between the two π-conjugated branches. These observations are fully supported by optical spectroscopic measurements (vide infra). After alkylation of the second pyridyl moiety, C_{2V} molecular symmetry is reestablished and the corresponding ^{1}H NMR spectra exhibit a single set of signals displaced to low-fields. The ^{1}H NMR spectra of chromophores **2**, **4**, and **6** are shown in Figure 1B. Neutral and dialkylated symmetric systems **2** and **6** exhibit a single set of resonances for the pyridine and pyridiniumethylene groups. The ^{1}H NMR spectrum of monoalkylated system **4** exhibits two sets of low-field shifted resonances. In system **4**, the π-conjugation extends throughout the entire molecule, corroborating substantial coupling between the formally neutral and formally charged molecular fragments.

The crystal structure of compound **2** and the adapted numbering scheme are shown in Figure 2. Single crystals were obtained by slow evaporation of a chloroform solution at room temperature. The crystal structure provides information on the molecular geometry and key bond lengths, affording a better understanding of the film microstructure. Cell constants and the orientation matrix for data collection correspond to an orthorhombic cell (*Pbca* space group, see the Supporting Information) with the following dimensions: $a = 17.945(10)$ Å; $b = 7.785(4)$

(17) (a) Nijmeijer, A.; Kruidhof, H.; Bredesen, R.; Verweij, H. *J. Am. Ceram. Soc.* **2001**, *84*, 136. (b) Krongelb, S. *Electrochem. Technol.* **1968**, *6*, 251.

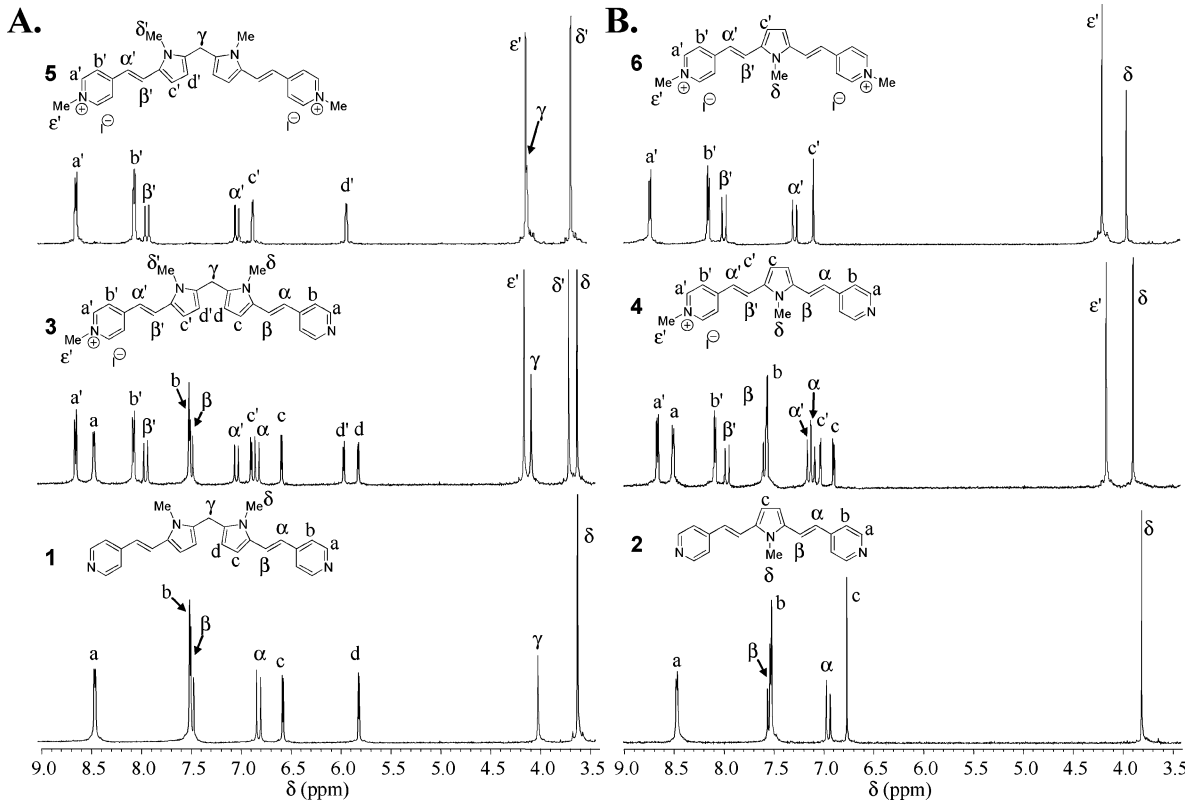

Figure 1. ^{1}H NMR spectra (300 mHz) of (A) **1** and of the corresponding mono- and dimethylated salts **3** and **5** and (B) **2** and of the corresponding mono- and dimethylated salts **4** and **6** in DMSO-d_6.

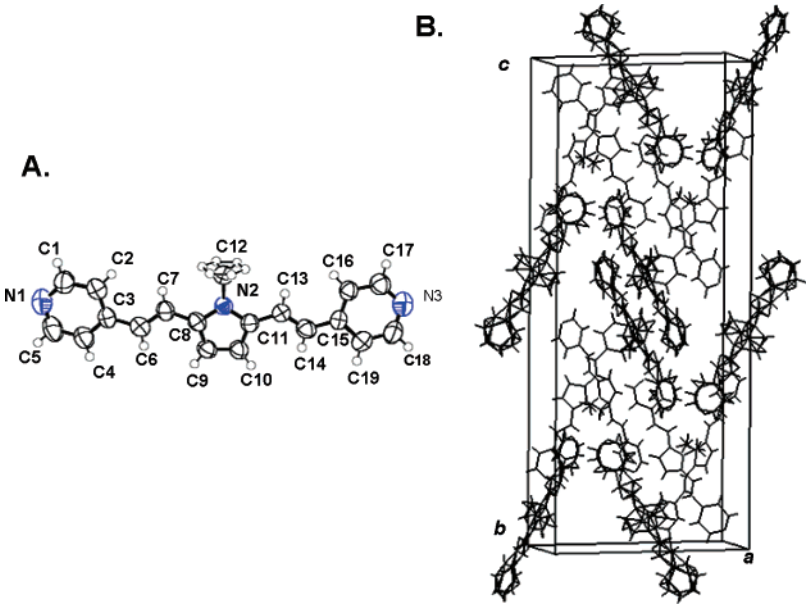

Figure 2. (A) Molecular structure and (B) packing diagram of molecule **2**.

Å; c = 43.07(3) Å; $\alpha = \beta = \gamma = 90°$. The maximum π-core length and width of the pyridine-pyrrole precursor **2** are ~ 15.31 Å (N1−N3) and 3.64 (C9−C12), respectively. The estimated length of parent compound **7** should then be comparable to that of the pyridine-ethylene-pyrrole fragment and is found to be ~8.8 Å (N1−C11 or N3−C8). The molecular structure of **2** reveals an essentially planar core with maximum pyridine−ethylene torsional angle of ~15°. These angles are considerably smaller than 30°, which is the maximum for which efficient intramolecular $\pi-\pi$ overlap can be achieved.[18] Compound **2** exhibits a *trans* conformation of the two double bonds connecting the pyrrolyl ring to the ethene bridges. The internal ring geometries of both pyridyl (~1.33 Å for C−N bonds and ~1.39 Å for C−C bonds) and pyrrolyl rings (~1.39 Å for all skeletal bonds) are unexceptional for substituted pyridine and pyrrole molecules.[19] The packing of **2** is complex, with the molecular

(18) (a) McCullough, R. D. *Adv. Mater.* **1998**, *10*, 93. (b) Brédas, J.-L. *J. Chem. Phys.* **1985**, *82*, 3809.
(19) Katritzky, A. R. *Handbook of Heterocyclic Chemistry*; Pergamon Press: Oxford, 1983.

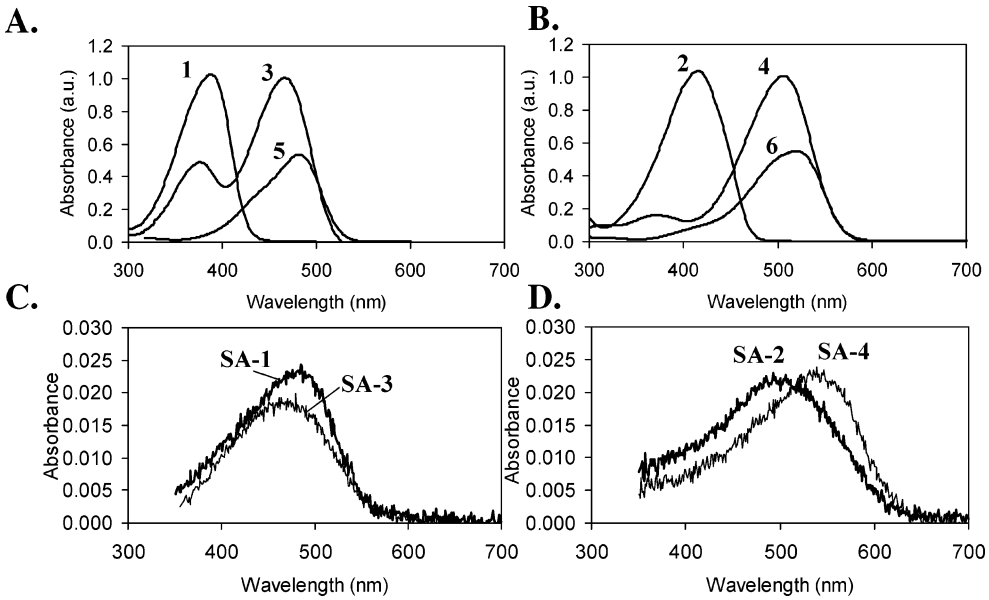

Figure 3. Optical absorption spectra of (A) MeOH solution of molecules **1**, **3**, and **5** at 25 °C. (B) MeOH solution of molecules **2**, **4**, and **6** at 25 °C. (C) Films **SA-1** and **SA-3**. (D) Films **SA-2** and **SA-4**.

Table 1. Optical Absorption and Emission Data of Compounds **1**−**8** and Self-Assembled Films **SA-1**−**SA-4** and **SA-7**

	absorption					emission		
	λ_{max} (nm)					λ_{max} (nm)		
compd/film	toluene	MeOH (ϵ)[a]	H_2O	film	$\Delta\lambda$[b]	ROH	film	$\Delta\lambda_s$[c]
1	374	387 (60050)			+13	458		81
3		465 (39200)	445		−20	520		75
5		478 (84400)	462		−16	533		71
SA-1				480			544	64
SA-3				468			525	57
2	404	415			+11	490		75
4		506	480		−26	587		107
6		520 (43600)	501		−19	593		92
SA-2				496			564	68
SA-4				537			601	64
7	356	362 (21100)			+6			
8		440 (39900)	420		−20	519		79
SA-7				448		525		77

[a] ϵ in l mol^{-1}cm^{-1}. [b] $\Delta\lambda = \lambda_{max}$ (solvent 1) − λ_{max} (solvent 2), $\epsilon_1 > \epsilon_2$: positive $\Delta\lambda$ mean positive solvatochromism. [c] Stock shift.

units preferentially aligned with the long axes parallel to *c* and stacking, in a slipped x-type herringbone fashion, in the *b* direction. The minimum intermolecular distance is ∼3.8 Å.

Chromophore and Film Linear Optical Characterization. UV−vis optical spectroscopy is used to assess the electronic effects of precursor **1** and **2** alkylation in solution and to characterize the functionalized substrate surfaces. The absorption spectra of compounds **1**−**7** and of films **SA-1**−**SA-4** and **SA-7** are shown in Figure 3. UV−vis data (λ_{max}, ϵ) for compounds **1**−**8** in methanol and either toluene or water are summarized in Table 1. Previous studies on azine-(π-conjugated)-excessive heterocyclic systems indicated that the neutral precursors such as **7** exhibit marginal push−pull activity compared to the corresponding pyridinium salt **8**. Therefore, **1** and **2** are expected to exhibit relatively small solvatochromic responses. On the other hand, alkylation of the pyridyl moiety is found to have a substantial influence on chromophore optical properties. In this case, however, it is found that the line shapes of the optical spectra and the extent of the absorption shift are closely related to the precursor molecular structure. Indeed, the UV−vis spectra of neutral precursors **1** and **2** and dimethyl salts **5** and **6** exhibit a single charge-transfer (CT) excitation indicative of either a single or of two identical chromophoric regions as in the case of **1** and **5**. However, monomethyl salts **3** and **4** behave differently.

The optical absorption spectrum of salt **3** exhibits two CT transitions centered at 370 and 478 nm which are associated with the neutral and charged molecular fragments, respectively. In contrast, the monomethyl iodide **4** exhibits a strong single CT band in agreement with delocalization of the entire chromophore π system. In all cases, CT features associated with the positively charged fragments are bathochromically shifted ($\Delta\lambda_n^+$)[20] compared to the neutral precursors **1** and **2**, due to the greater acceptor capacities of pyridinium vs pyridyl groups. In methanol, this effect is larger for derivatives **4** and **6** ($\Delta\lambda_n^+$ = 91/105 nm for **2** → **4**/**6**) than for salts **3** and **5** ($\Delta\lambda_n^+$ = 78/91 nm for **1** → **3**/**5**). The established correlation between donor/acceptor strength and $\Delta\lambda_n^+$ suggests that in the present chromophores, intramolecular charge transfer[19] increases with increasing donor/acceptor strength. Since in this case the donor and acceptor units are identical, the increased polarizabilities of **4** and **6** are the result of an increased number of delocalized π electrons, hence extension of the effective conjugation length. The same conclusion can be drawn by analyzing the solvatochromic responses ($\Delta\lambda$) of these systems. The respective solvatochromic responses are larger for chromophore pairs **4** (−26 nm) and **6** (−19 nm) than for pairs **3** (−20 nm) and **5** (−16 nm). As expected, neutral precursors **1** and **2** exhibit far smaller $\Delta\lambda$ parameters (+13 nm and +11 nm, respectively), in agreement with the decreased tendency of the pyridyl group to function as an acceptor. Table 1 also summarizes chromophore/film emission data in anhydrous methanol and shows that quaternization of azine nitrogen also has a dramatic influence on the fluorescence properties of these heterocycle-based systems. All systems emit in the visible region (458−593 nm) when excited at their absorption maxima. However, although

(20) The parameter $\Delta\lambda_n^+ = (\lambda_{max})_{cation} - (\lambda_{max})_{neutral}$ is defined as the difference between the ICT band value of the methylazinum ion and that of the corresponding azine base. See ref 16a.

PL quantum efficiency was not measured, the neutral systems **1** and **2** exhibit much lower emission intensity than the corresponding salts. Combining absorption and emission data, the HOMO−LUMO (optical) energy gap can be estimated to be in the range of 2.2−2.5 eV for all of the present chromophores in solution. Comparable values are found for the corresponding SA films (vide infra).

For the chemisorbed systems, optical spectroscopic data provide strong evidence of monolayer formation and preferential chromophore orientation (Figure 3). Thus, the colorless benzylhalide-functionalized glass slides (**SA-IBnS**) become light-orange (**SA-1** and **SA-3**), deep-red (**SA-2**), and purple (**SA-4**) after reaction with the respective chromophore precursors. The optical absorption spectra of all chromophoric monolayers exhibit a single CT feature (480 nm, **SA-1**; 468 nm, **SA-3**; 496 nm, **SA-2**; 537 nm, **SA-4**) centered in the absorption region of salts **3-6** in MeOH. The presence of a single absorption band in the spectrum of **SA-1**, centered very close to the absorption maximum of dimethyl salt **5**, indicates that predominantly both pyridine moeities of precursor **1** undergo reaction with the functionalized surface. Monoalkylation would afford one neutral pyridylpyrrole fragment and consequently a second absorption of roughly similar intensity ratio, as found in solution for **3**, would be expected in the ∼380 nm region. Furthermore, the similarity between the optical spectra of **SA-1** and **SA-3** ($\Delta\lambda_{max}$ = 12 nm) argues that the molecular electronic structure of **SA-1** is very similar to that of the dialkylated **SA-3** monolayer. Film spectra of **SA-2** and **SA-4** provide less structural information since both mono- and dimethyl salts **4** and **6** exhibit a single, energetically similar absorption maximum. However, **SA-2** λ_{max} is considerably blue- shifted with respect to **6**. These observations and the large difference between **SA-2** and **SA-4** absorption maxima ($\Delta\lambda_{max}$ = 41 nm) suggest that chemisorption by monoalkylation of **2** cannot be ruled out. The optical data also highlight a different reaction pattern between fully conjugated chromophores **2** and **4** vs methylene-bridged molecules **1** and **3**. For both systems, it is expected that chemisorptive monoalkylation would bring the second chromophore moiety in close proximity to the benzyl halide surface. A consecutive quaternization process then seems more likely than reaction of the benzyl halide terminated surface with another incoming chromophore. However, the ^{1}H NMR and optical spectroscopic data in solution show that monoalkylation of conjugated chromophore **2** significantly reduces the electron density of the second pyridyl group, whereas monolalkylation of **1** does not appreciably affect the electron density of the second chromophore fragment. Thus, in the case of **2**, the first chemisorptive alkylation deactivates the second pyridyl moiety, resulting in films with both mono- and dialkylated chromophores. However, for **1**, the first alkylation step does not deactivate the second pyridyl moiety and results in a more homogeneous film structure. These assertions are supported by XPS and XRR data (vide infra).

Film Microstructural Characterization and Electrooptic Response. (1) Atomic Force Microscopy and X-ray Photoelectron Spectroscopy. Noncontact mode AFM measurements were performed on all SA films. This study reveals similar topographies with the formation of relatively smooth and homogeneously covered surfaces, without obvious cracks or pinholes. Representative AFM images of **SA-1** and **SA-2** over

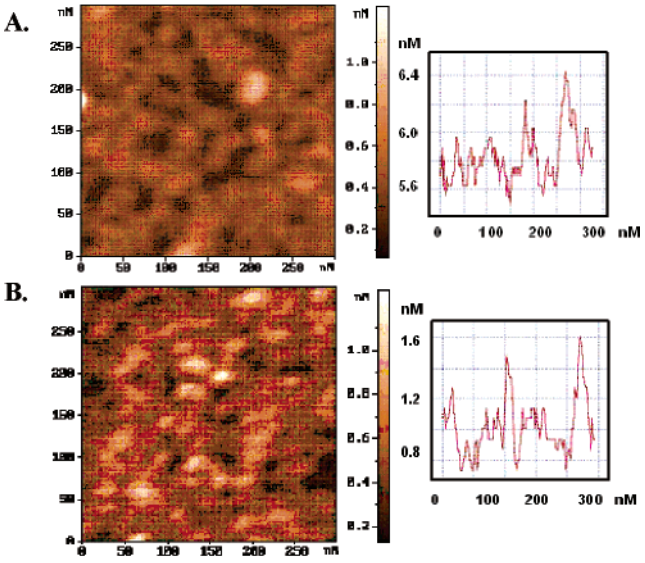

Figure 4. AFM images of 0.3 μm × 0.3 μm scan areas for (A) **SA-1** and (B) **SA-2**. AFM cross-sections of the corresponding films on Si(100) are shown on the right side. Films were prepared by solution deposition.

0.3 × 0.3 μm scan areas and cross-sections of the corresponding films on Si(100) are shown in Figure 4. Films of the coupling reagent **SA-IBnS** (not shown) exhibit an RMS surface roughness < 0.2 nm. The typical step-size of the molecular assemblies of **SA-1** revealed by NC-AFM is about 0.4−0.6 nm, whereas those of **SA-2**−**SA-4** are slightly greater (0.6−1.0 nm), in agreement with the molecular dimensions and inherent surface roughness.

XPS studies were performed on **SA-1**−**SA-4** films grown on n-type silicon and confirm the presence of the expected elements such as Si, O, C, N, and I. Particularly interesting are the high-resolution XPS nitrogen (1s) signals for the **SA-1**−**SA-4** samples, which are shown in Figure 5. Included in the figure are the results of the curve resolution analysis for N(1s) features. The ionizations at 398.8, 400.2, and 402.6 (±0.1) eV were used in the deconvolution process, and correspond to energies characteristic of pyridinic, pyrrolic and quaternary-type nitrogen functionalities, respectively.[21] In each case, the N(1s) signal was analyzed using a 70% Gaussian 30% + Lorentzian line shape and a peak fwhm of 1.7 (eV) for each signal; these are the same parameters used to fit individual nitrogen functionalities in model compounds. The peak shape and peak energy positions are fixed in the curve resolution process adopted in the present study, and only the amplitudes of these peaks were varied to obtain the best fit to the experimental XPS data. It is important to emphasize that quantification of nitrogen forms based on the XPS curve resolution is very sensitive to the signal-to-noise characteristics of the XPS spectrum. In the present study, the signal-to-noise ratio is insufficient for a fully quantitative data analysis. However, in all cases the XPS measurements reveal the presence of all of the expected N(1s) signals. Interestingly, deconvolution of powder XPS data on microanalytically pure samples of chromophores **5** and **6**, which should not exhibit any neutral pyridine N(1s) signals, also reveals the presence of three N(1s) signals (not shown) at the same binding energies. This result suggests that the interpretation of these XPS data is not straightforward and requires additional study. A possible reason for the presence of all signals may be due to the fact

(21) *Surface Analysis by Auger and X-ray Photoelectron Spectroscopy*; Briggs, D., Grant, J. T., Eds.; IM Publications: Chichester, U.K., 2003.

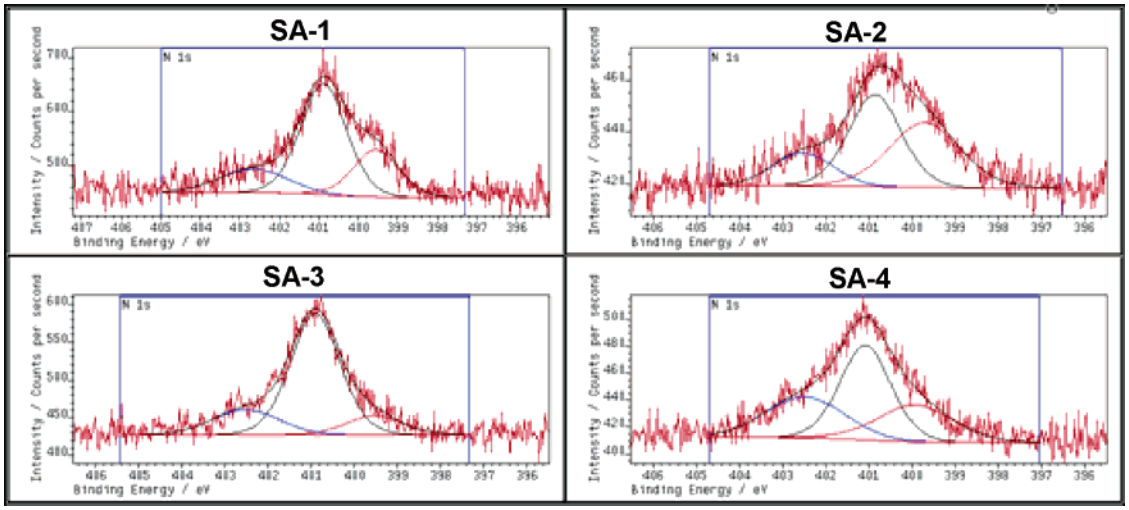

Figure 5. Representative N(1s) XPS data for films **SA-1**−**4**.

that these chromophores are, after alkylation/reaction with the surface, merocyanines and therefore should exhibit considerable electron density transfer from the pyrrolyl to the pyridinium nitrogen. Therefore, the actual electronic structure of the molecular ground state of these systems is not that of a simple pyridinum−ethene−pyrrole framework but rather a resonance hybrid of the two limiting **A** and **B** structures.

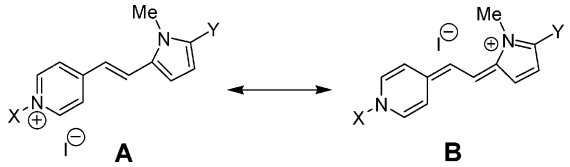

X = Me, substrate surface; Y = remaining molecular fragment

Upon charge transfer, the pyridinium N acquires enaminic character, whereas the pyrrole N becomes immonium-like, thereby inducing significant shift in the N(1s) binding energies. The extent of charge transfer and therefore the relative **A** vs **B** contribution is strongly affected not only by the nature of the donor/acceptor groups but also by environmental polarity, counterion location, and local molecular packing/conformations. All of these may vary considerably within the films. Similar complex XPS spectra presenting difficulties in straightforward interpretation have been observed for other cyanine dyes as powder and as thin LB film samples[22] as well as for electrochemically synthesized polypyrrole and polyaniline films.[23] Despite these uncertainties there are important differences between the XPS signatures of **SA-1** and **SA-3**, as well as between **SA-2** and **SA-4**, which clearly result from different molecular structures of the neutral (**1** and **2**) versus the monomethylated salt (**3** and **4**) monolayer precursors. In fact, while **SA-1** and **SA-2** should have a certain degree of free "pyridine-like" N character, depending on the efficiency with which the second pyridine of the molecule undergoes reaction with the **SA-IBnS** surface, this is chemically impossible for stoichiometrically precise **SA-3** and **SA-4** films. In agreement with this observation, the XPS spectra of **SA-3** and **SA-4** reveal a significantly weaker signal at 398.8 eV, suggesting that the unreacted "neutral" pyridine content is diminished, as expected. Furthermore, the XPS spectra of **SA-1** exhibit a relative reduction of the "neutral" N(1s) signal compared to that of **SA-2**, suggesting that the second alkylation is much more effective for **1** than for **2**, in very nice agreement with the results of the other film characterization techniques.

(2) Synchrotron X-ray Reflectivity. X-ray reflectivity measurements were performed on films **SA-1**−**SA-4** which were prepared on the native oxide surface of polished single-crystal Si(100) wafers. Figure 6 shows the reflectivity data normalized to the Fresnel reflectivity for all films. The reflected intensity was measured as a function of the scattering vector perpendicular to the reflecting surface. A Gaussian-step model was used to fit the specular reflectivity data to obtain key film microstructural parameters such as the film thickness (d) and the root-mean-square width of each interface, including $\sigma_{\text{film-air}}$ which corresponds to the film roughness. The chromophore number density (N_s) and the molecular footprint (MFP) were also calculated from the electron density per unit area for a single molecular layer. The latter was obtained from the XRR-derived electron density profile and the number of electrons for each SA molecule, calculated from the chemical formula of films **SA-1**−**SA-4**. A detailed description of the XRR data analysis and model employed can be found elsewhere.[20]

The XRR data presented in Table 2 are the results of three independent sets of measurements. For comparison, the previously reported self-assembled film of precursor **7** (**SA-7**, not shown in Scheme 4) was prepared under identical reaction conditions and also analyzed by XRR. The film thicknesses of methylene-spaced SAMs **SA-1** and **SA-3** are in the same range as that of **SA-7** (∼13 Å), and all samples are comparably smooth. These dimensions are in agreement with the expected molecular geometries of the SAMs, composed of a coupling layer (**SA-BnS**) of ∼6.5 Å thickness and a pyridinium−ethene−pyrrole fragment of ∼9 Å, as indicated from the crystal structure of **2**. However, note that **SA-3** is more than 1 Å thicker than **SA-1**, probably because to accommodate the V-shaped molecular structure ending in a *N*-methylpyridinium group, steric

(22) (a) Xu, T.; Morris, T. A.; Szulczewski, G. J.; Amaresh, R. R.; Gao, Y.; Street, S. C.; Kispert, L. D.; Metzger, R. M.; Terenziani, F. *J. Phys. Chem. B* **2002**, *106*, 10374. (b) Botelho do Rego, A. M.; Penedo Pereira, L.; Reis, M. J.; Oliveira, A. S.; Vieira Ferreira, L. F. *Langmuir* **1997**, *13*, 6787.

(23) (a) Wong, K. Y.; Smallfield, J. A. O.; Fahlman, M.; Epstein, A. J. *Synth. Met.* **2003**, *137*, 1031. (b) Nicolau, Y. F.; Ermolieff, A. *Synth. Met.* **1995**, *72*, 2073. (c) Benseddik, E.; Makhlouki, M.; Bernede, J. C.; Lefrant, S.; Pron, A *Synth. Met.* **1995**, *72*, 237. (d) Inoue, M. B.; Nebesny, K. W.; Fernando, Q.; Inoue, M. *J. Mater. Chem.* **1991**, *1*, 213.

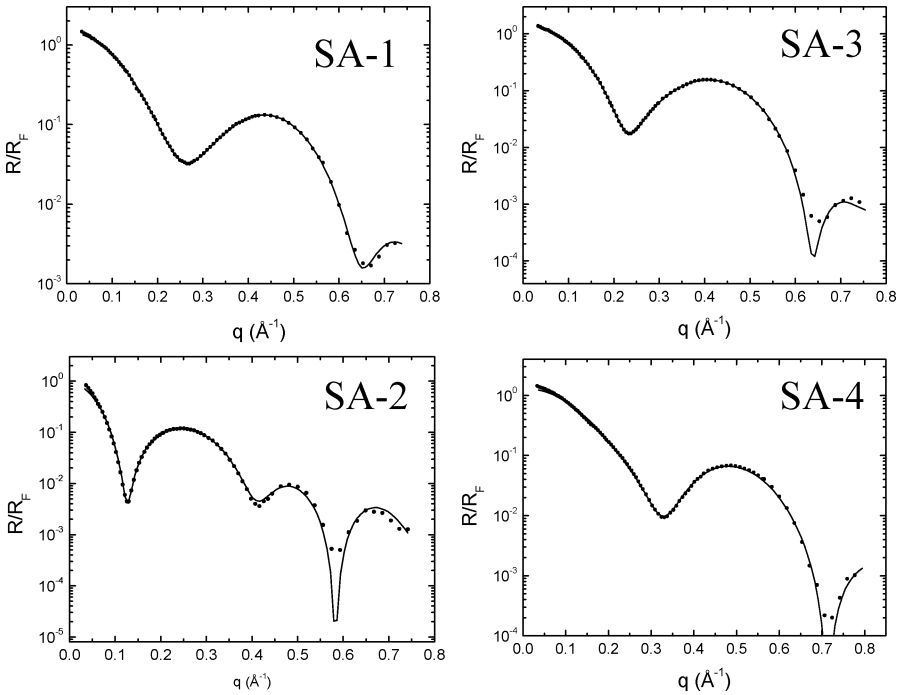

Figure 6. X-ray reflectivity data normalized to the Fresnel reflectivity R_F plotted versus scattering vector component, q_z, for films **SA-1**−**SA-4**. Solid lines: best fits based on one-layer (**SA-1**, **SA-3**, **SA-4**) and two-layer (**SA-2**) Gaussian-step models.

Table 2. Specular XRR[a] and SHG (λ = 1064 nm) Data for Self-Assembled Films of Chromophores **1**−**4** and **7**

					spin coating		solution deposition	
film	d (Å)	$\sigma_{film-air}$ (Å)	MFP (Å^2)	N_s, × 10^{14} (molecules/cm^2)	$\chi^{(2)}$	r_{33}[b]	$\chi^{(2)}$	r_{33}[b]
SA-1	12.4 ± 0.2	3.6 ± 0.2	73	1.4	210	64	49	15
SA-3	13.5 ± 0.2	3.7 ± 0.2	65	1.5	35	11	6	2
SA-2	21 ± 1	8 ± 1	∼ 50	∼ 2	76	23	7	2
SA-4	10.5 ± 0.2	3.6 ± 0.2	66	1.5	16	5	<1	<1
SA-7	13.3 ± 0.2	3.6 ± 0.2	46	2.2	142	44	44	13

[a] d = film thickness; $\sigma_{film-air}$ = film roughness; MFP = molecular footprint; N_s = chromophore density for spin-coated films. [b] r_{33} is estimated at 1064 nm from $(2 \times \chi^{(2)})/n^4$ with n = 1.6 (Ashley, P. R.; Cites, J. S. *Opt. Soc. Am. Technol. Digest Ser.* **1997**, *14*, 196).

hindrance forces the chromophore further from the substrate surface (see Scheme 4). With respect to monomeric precursor **7**, note that the larger adsorbate molecules **1** and **2** are expected to occupy more area on the substrate surface. Indeed, the molecular footprints of **SA-1** and **SA-2** are ∼30% larger than that of **SA-7** and consequently, their number density is found to be less. More complex is the comparative analysis of the XRR data for films **SA-2** and **SA-4**. The former is two times thicker (∼21 Å) than **SA-4** (10.5 Å) and all of the other chromophore SAMs. A single-layer Gaussian-step model does not yield a convincing fit, indicating that this system has a complicated electron density profile. In addition, the corresponding one-dimensional Patterson function calculated from the reflectivity data shows, without any model-dependent assumptions, that there is a clear density variation within the film. Assuming the presence of two different regions having different electron densities within the film, we obtain a good fit to the data (solid line in Figure 6 for the sample **SA-2**). Combining this information with the relatively large film roughness (∼8 Å) and high chromophore density, it is suggested that **2** undergoes reaction with the **SA-IBnS** surface to yield a mixture of mono- and dianchored chromophores. This model is in good agreement with the optical spectroscopic measurements discussed above. Furthermore, it is expected that reaction of both pyridyl groups with the coupling layer would necessarily lead to much thinner films. On the other hand, if **2** chromophores were only singly anchored to the surface, the measured film thickness of 21 Å is in the expected range (coupling layer thickness + length of **2** = 6.5 + 15.3 Å). The estimated chromophore footprint of **SA-2** ∼ 50 Å^2 is comparable to the dimensions of chromophore **2** (15 × 3.6 = 54 Å^2) estimated from the crystal structure. The $\sigma_{film-air}$ of ∼8 Å, which is in the same dimensional range as the pyridine-ethene-pyrrole moiety, argues for a mixture of singly and a doubly anchored chromophore units (see **SA-2** in Scheme 4). The remaining question is why the **SA-3** and **SA-4** films are thin and smooth although the corresponding singly anchored systems could in principle assume a variety of conformations on the substrate surface. A possible explanation is related to the tendency of polar/ionized species to remain closer to the polar bulk and to minimize surface area at the film-air interface. Such arrangements are known to strongly reduce film surface free energy.[24]

(3) Second-Harmonic Generation Spectroscopy. Figure 7 shows the angle-dependent intensity of second-harmonic light generated from the interaction of the incident laser beam (λ_0 =

(24) (a) Etzler, F. M. *Contact Angle, Wettability Adhes.* **2003**, *3*, 219. (b) Chibowski, E.; Perea-Carpio, R. *Adv. Colloid Interface Sci.* **2002**, *98*, 245. (c) Ulman, A. *Thin Solid Films* **1996**, *273*, 48. (d) Ryntz, R. A. *Prog. Org. Coatings* **1994**, *25*, 73. (e) Kloubek, J. *Adv. Colloid Interface Sci.* **1992**, *38*, 99. (f) Sato, T.; Tsugaru, T.; Yamauchi, J.; Okaya, T. *Polymer* **1992**, *33*, 5066.

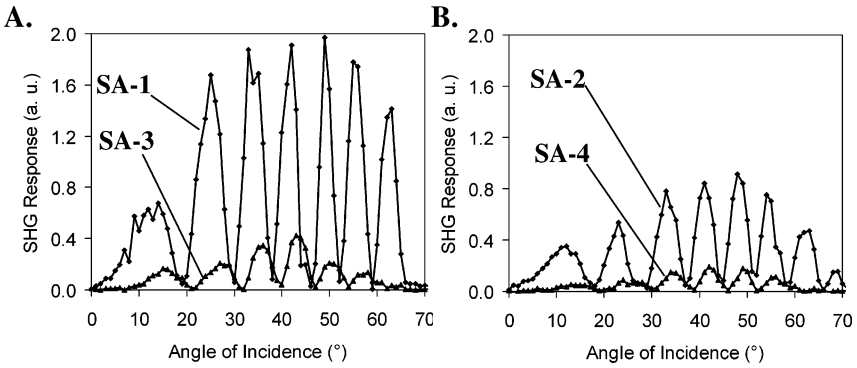

Figure 7. Intensity of SHG signal (arbitrary units) as a function of the fundamental beam incident angle from a float glass slide having films **SA-1**,**3** and **SA-2**,**4** on either side.

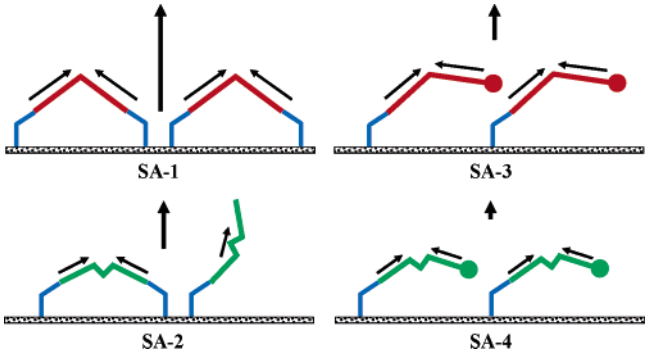

Figure 8. Schematic representation of the bulk (thick arrows) and local (thin arrows) dipole moments of films **SA-1**−**SA-4**. Blue lines represent the coupling layer, red lines represent chromophores of type **1** and **3**, green lines represent chromophores of type **2** and **4**, and the filled ring represent charged pyridinium/iodide end groups.

1064 nm) with a glass slide coated on both sides with the chromophore monolayers **SA-1**−**SA-4**. These measurements provide additional insight into film microstructure and bulk polarity. The characteristic second-harmonic generation (SHG) interference pattern with near-zero intensity minima arising from the phase difference between the two SHG waves generated at either side of the sample indicates an identical and uniform coating on both sides of the glass substrate. Table 2 also summarizes the bulk second-order nonlinear susceptibility ($\chi^{(2)}_{zzz}$) and the electrooptic coefficient (r_{33}) for **SA-1**−**SA-4** and **SA-7**, obtained by calibration of the SHG data against quartz. Remarkably, the SHG data show that films prepared by chromophore spin-coating and vacuum oven treatment exhibit significantly larger NLO responses than films prepared by the solution-based deposition method. In accord with these results, the optical spectra of the solution-prepared films (not shown) are much weaker and broader than those fabricated via the spin-coating/vacuum-oven method, suggesting a lower chromophore density.

The second-order NLO response of **SA-1** (210 pm/V at 1064 nm) is the highest of the films in the present study and larger than that of the previously reported monomer chromophore-based **SA-7** film (142 pm/V).[16] Since **1** and **7** have identical donor and acceptor components, the ∼50% increase in $\chi^{(2)}$ response of **SA-1** versus **SA-7** must be the result of a different film microstructure (Figure 8). The XRR measurements demonstrate that the surface molecular density of **SA-1** is somewhat lower than that of **SA-7** (1.4 vs 2.2 × 10^{14} molecule/cm^2). However, this corresponds to an actual increase of the NLO-phore units in **SA-1** by ∼30%, since **1** consists of two chromophore units. The second contribution, which must account for an additional 20% increase, is due to improved overall film polar order. The double anchorage to the surface likely decreases the dispersion of the molecular dipole orientations along the substrate normal and consequently increases bulk polar order. Finally, a minor contribution to the increased response of **SA-1** may be provided by the increased donor capacity of an alkyl-substituted pyrrole (the CH_2 group of **1** acts as a $+I$ group) versus the unsubstituted ring of **7**. This result is also supported by the bathochromic shift and enhanced solvatochromic response of **1** and **3** (alkyl substituted chromophores) compared to **7** and **8**, respectively. The NLO responses of the other films (**SA-3**, 35 pm/V; **SA-2**, 76 pm/V; **SA-4**, 16 pm/V) are far lower than those of **SA-1** (210 pm/V) and **SA-7** (142 pm/V). Among them, **SA-2** exhibits the largest coefficient, which corroborates the film microstructure model as a mixture of singly and doubly anchored chromophores. In fact, since **SA-4** exhibits the smallest $\chi^{(2)}$ (Table 2) it is expected that a completely doubly anchored monolayer of chromophore **2** should also exhibit very poor second-order response. In such films, the average component of the molecular dipoles along the substrate normal should be almost zero since the chromophore is expected to lie nearly flat on the substrate surface. Therefore, the response of **SA-2** derives principally from singly anchored chromophores, which extend along the substrate normal. To a first approximation, the molecular hyperpolarizability β of the monomethyl salts **4** and **8** should be comparable since their solvatochomic responses ($\Delta\lambda = -26$ and -20 nm) are similar. Interestingly, the $\chi^{(2)}$ response of **SA-2** is about 50% of the $\chi^{(2)}$ of **SA-7**, although both films exhibit similar chromophore surface coverage (∼2 × 10^{14} molecules/cm^2), suggesting that the ratio between the singly and doubly anchored chromophores in **SA-2** is near unity. The NLO responses of singly anchored chromophore films **SA-3** and **SA-4** are very small. This result is clearly not due to the poor molecular hyperpolarizabilities of the constituent chromophores. Rather, the geometries of the assembled molecules and the film microstructure must generate an averaged centrosymmetric charge distribution which dramatically reduces the second-order response. These systems are therefore attractive for applications where large polarizations are associated with symmetric intramolecular CT, such as third-order NLO processes. Indeed, we recently reported promising results in this direction and further studies are in progress.[16d]

Conclusions

The synthesis and physicochemical properties of several new heterocycle-based "push−pull" chromophore systems is described. The reaction of pyrrole derivative **7** using a Mannich protocol strongly depends on the presence of H_2O. The resulting mono- (**7**) and new dimeric chromophore (**1**, **2**) precursors can be mono- and dialkylated to afford the corresponding *N*-monomethyl- (**3**, **4**, **8**) and *N*,*N*′-dimethyl iodide salts (**5**, **6**). Chromophore precursors **1** and **2** and the corresponding *N*-monomethyl salts **3** and **4** undergo reaction with iodobenzyl-functionalized surfaces to afford σ-bonded self-assembled films. The film microstructure and the corresponding EO response are substantially affected by the design of the molecular precursors and the film deposition method. Thus, spin-coating of the chromophore precursors on a benzyl-halide functionalized substrate-surface followed by a vacuum oven treatment results in films with far larger NLO responses (up to 1 order of magnitude) than films prepared by a stepwise solution-based assembly process. The second-order NLO response of **SA-1** is far larger than that of **SA-2**, indicating that these systems have substantially different film microstructures and π-electron distributions. Indeed, given that both pyridyl rings undergo reaction with the coupling layer, the methylene-bridge in **1** blocks π-conjugation and allows formation of an effective push−pull, asymmetric spacer-(D-π-*A*)$_2$. On the other hand, system **2** affords a mixture of singly- and doubly anchored chromophore structures, the latter having a significantly weaker asymmetric push−pull activity. These SA chromophoric films therefore exhibit complementary nonlinear optical properties and have potential for NLO/EO applications.

Acknowledgment. This research was supported by the NSF-Europe Program (DMR-0353831), ARO/DARPA (DAAD 19-00-1-0368), the ISF-BIKURA program, MJRG, and by CNR-progetto finalizzato MSTA II. We thank the Northwestern MRSEC for access to characterization facilities supported under Grant No. DMR-0076097. X-ray reflectivity measurements were performed at Beam Line X23B of the National Synchrotron Light Source, which is supported by the U.S. Department of Energy. A.S. is the recipient of The Reva G. Stone Postdoctoral Fellowship. M.E.v.d.B. is the incumbent of the Dewey David Stone and Harry Levine Career Development Chair and thanks the Israeli Council for Higher Education for an Alon Fellowship. We thank Dr. Y. Feldman and Dr. H. Cohen (WIS) for their valuable assistance in the AFM and XPS measurements, respectively.

Supporting Information Available: General procedures, chromophore synthetic details amd characterization, and film self-assembly procedure. X-ray data of **2** (CIF). This material is available free of charge via the Internet at http://pubs.acs.org.

JA057556C